

A short-period super-Earth orbiting the M2.5 dwarf GJ 3634^{★,★★}

Detection with HARPS velocimetry and transit search with *Spitzer* photometry

X. Bonfils^{1,2}, M. Gillon^{2,3}, T. Forveille¹, X. Delfosse¹, D. Deming⁴, B.-O. Demory⁵, C. Lovis², M. Mayor²,
V. Neves^{1,6}, C. Perrier¹, N. C. Santos^{6,7}, S. Seager⁵, S. Udry², I. Boisse⁶, and M. Bonnefoy¹

- ¹ UJF-Grenoble 1/CNRS-INSU, Institut de Planétologie et d'Astrophysique de Grenoble (IPAG) UMR 5274, 38041 Grenoble, France
e-mail: Xavier.Bonfils@obs.ujf-grenoble.fr
² Observatoire de Genève, Université de Genève, 51 Ch. des Maillettes, 1290 Sauverny, Switzerland
³ Institut d'Astrophysique et de Géophysique, Université de Liège, Allée du 6 Août 17, Bât. B5C, 4000 Liège, Belgium
⁴ Planetary Systems Branch, Code 693, NASA/Goddard Space Flight Center Greenbelt, MD 20771, USA
⁵ Department of Earth, Atmospheric and Planetary Sciences, Department of Physics, Massachusetts Institute of Technology,
77 Massachusetts Ave., Cambridge, MA 02139, USA
⁶ Centro de Astrofísica, Universidade do Porto, Rua das Estrelas, 4150-762 Porto, Portugal
⁷ Departamento de Física e Astronomia, Faculdade de Ciências, Universidade do Porto, Portugal

Received 22 October 2010 / Accepted 19 January 2011

ABSTRACT

We report on the detection of GJ 3634b, a super-Earth of mass $m \sin i = 7.0_{-0.8}^{+0.9} M_{\oplus}$ and period $P = 2.64561 \pm 0.00066$ day. Its host star is a M2.5 dwarf, has a mass of $0.45 \pm 0.05 M_{\odot}$, a radius of $0.43 \pm 0.03 R_{\odot}$ and lies 19.8 ± 0.6 pc away from our Sun. The planet is detected after a radial-velocity campaign using the ESO/HARPS spectrograph. GJ 3634b had an a priori geometric probability to undergo transit of $\sim 7\%$ and, if telluric in composition, a non-grazing transit would produce a photometric dip of $\lesssim 0.1\%$. We therefore followed-up upon the RV detection with photometric observations using the $4.5\text{-}\mu\text{m}$ band of the IRAC imager onboard *Spitzer*. Our six-hour long light curve excludes that a transit occurs for 2σ of the probable transit window, decreasing the probability that GJ 3634b undergoes transit to $\sim 0.5\%$.

Key words. techniques: radial velocities – stars: late-type – planetary systems

1. Introduction

The subset of extrasolar planets that transit their parent star have had the most impact on our understanding of their planetary structure and atmospheric physics (as reviewed by Charbonneau et al. 2007). They are the only ones for which one can simultaneously measure mass and radius, and, by inference, internal composition. The few that transit a host star bright enough for detailed spectroscopic follow-up provided additional observational information on the composition and physics of extrasolar planetary atmospheres, which opened the new scientific field of physical exoplanetology. That select group of very bright transiting systems, with transit depths deep enough for detailed characterization, only has a handful of members, and until recently all were gaseous giant planets. The recent discoveries that GJ 436b and GJ 1214b undergo transits (Gillon et al. 2007;

Charbonneau et al. 2009) has extended that new field to the realms of the ice giants and super-Earth planets.

To search for transiting planets, two strategies compete: the *photometric* and the *radial-velocity educated* approach. The photometric approach detects planets when they transit their parent star and, de facto, is the most direct strategy to find transiting planets. Alternatively however, one may wait for the detection of a planet before undertaking its photometric search for transit. If the planet is first detected, with the radial-velocity (RV) technique for instance, not only is the presence of the planet then known for sure, but the observational window to perform a photometric search is very much narrowed with an a priori ephemeris. This latter approach, though less direct, can prove more successful in finding planets that transit bright nearby stars, like for the “blockbusters” HD 209458b, HD 189733b and GJ 436b, which were first detected with RV measurements and then found to undergo transit with subsequent photometric campaigns.

During the first six years of HARPS operations, we ran a search for planets orbiting very-low-mass stars on guaranteed time observations. Our sample was composed of ~ 110 M dwarfs, and we have had success in finding 11 planets (Bonfils et al. 2005a, 2007; Udry et al. 2007; Mayor et al. 2009; Forveille et al. 2009, Delfosse et al., in prep.), although two were actually detected thanks to a complementary sample (Forveille et al. 2011).

* Based on observations made with the HARPS instrument on the ESO 3.6-m telescope at La Silla Observatory under program IDs 082.C-0718(B) and 183.C-0437(A), and observations made with *Warm Spitzer* under program 60027.

** Radial-velocity and photometric tables (Tables 2 and 3) are only available in electronic form at the CDS via anonymous ftp to cdsarc.u-strasbg.fr (130.79.128.5) or via <http://cdsarc.u-strasbg.fr/viz-bin/qcat?J/A+A/528/A111>

Among those detections, we count both the lowest-mass planet orbiting a main-sequence star known to date and the first prototypes of habitable planets (Udry et al. 2007; Mayor et al. 2009).

Most recently, we extended that initial sample to more than 300 M dwarfs. For all newly added stars, we focused on the detection of short period planets, with the goal to quickly identify the best candidates for a subsequent transit search.

In this paper, we report on the first detection obtained with that new sample and strategy, a super-Earth orbiting the M2.5 dwarf GJ 3634, and its search for transit with *Spitzer* photometry. The paper is structured as follows. In Sect. 2 we give the criteria of our extended sample and describe the stellar properties of GJ 3634. In Sect. 3 we present and analyze the RVs gathered on GJ 3634. We show their variation are compatible with a planet orbiting the star, plus a long-term drift that is indicative of an additional companion at larger separation. In the same section, we contemplate the possibility that the observed Doppler shifts could be faked by stellar surface inhomogeneities. We searched different stellar activity diagnostics for periodicities, but found no counterpart to the RV variation, which therefore strengthen the planetary interpretation. In Sect. 4, we present our photometric campaign that aimed to search for a possible transit. After considering the detection itself, we take a closer look at the non-detection limit in Sect. 5. Finally, Sect. 6 summarizes our results and discusses the prospects for the RV-educated approach to the search for planets that transit bright nearby stars.

2. Stellar properties of GJ 3634

GJ 3634 (aka LHS 2335) is an M2.5 dwarf (Hawley et al. 1996) seen in the Hydra constellation. It was first referenced by Eggen (1987) in a catalog of southern high proper motion stars and, according to Simbad, no more than five other times since. Riedel et al. (2010) recently reported a distance $d = 19.8 \pm 0.6$ pc ($\pi = 50.55 \pm 1.55$ mas) and an apparent brightness $V = 11.93 \pm 0.01$ mag. Together with a declination $\delta = -31.1^\circ$, GJ 3634 fulfills the criteria of our extended sample, which includes ~ 300 M dwarfs closer than 20 pc, brighter than $V = 12$ mag and southward of $\delta = 15^\circ$, as well as ~ 40 fainter stars kept from our initial sample ($V < 14$ mag; $d < 11$ pc; $\delta < 15^\circ$).

Its infrared photometry ($J = 8.361 \pm 0.023$ mag; $K = 7.470 \pm 0.027$ mag – Skrutskie et al. 2006) and parallax imply an absolute K -band magnitude $M_K = 5.99 \pm 0.16$ mag. Using the K -band mass-luminosity relationship of Delfosse et al. (2000) we attribute a mass $M_\star = 0.45 M_\odot$ to GJ 3634, to which we quote a 10% uncertainty. We estimate its luminosity $L_\star = 0.025 \pm 0.004 L_\odot$ after converting its absolute K -band magnitude to a bolometric magnitude using its $J - K$ color and Leggett (1992)'s bolometric correction ($BC_{K|J-K} = 2.74 \pm 0.07$ mag). The metallicity calibrations proposed in the recent years attribute a roughly solar metallicity to GJ 3634, with $[\text{Fe}/\text{H}] = -0.10$, $+0.15$ and $+0.01$ dex, following Bonfils et al. (2005b), Johnson & Apps (2009) and Schlaufman & Laughlin (2010), respectively. Assuming solar metallicity and an age of 5 Gyr, we also evaluate its radius $R_\star = 0.43 \pm 0.03 R_\odot$ from Baraffe et al. (1998)'s models, with an error estimate combining GJ 3634's K -band luminosity uncertainty to a model uncertainty of $\sim 5\%$. We note that for such a low-luminous star, Selsis et al. (2007) would place the habitable zone (defined as the region where liquid water can be stable on the surface of a rocky planet; Kasting et al. 1993) at a distance between 0.12 and 0.33 AU.

To assess GJ 3634's activity level we look at the Na I doublet. This is known to be an equivalent diagnostic to Ca II H&K emission lines and a more adequate choice when blue-most spectral

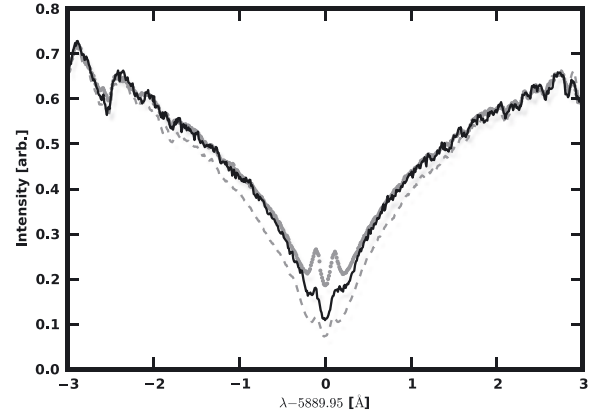


Fig. 1. Comparison of Na I D lines for three M2.5 dwarfs, from top to bottom, GJ 176 (gray dots), GJ 3634 (black line) and GJ 581 (gray dashes).

Table 1. Observed and inferred stellar parameters for GJ 3634.

Parameters	GJ 3634
α	$10^{\text{h}}58^{\text{m}}35.10^{\text{s}} \dagger$
δ	$-31^{\circ}08'39.1'' \dagger$
Spectral type	M2.5
π	50.55 ± 1.55 [mas]
d	19.8 ± 0.6 [pc]
V	11.93 ± 0.01 [mag]
M_V	10.45 ± 0.15 [mag]
K	7.470 ± 0.027 [mag]
M_K	5.99 ± 0.16 [mag]
L_\star	0.020 ± 0.002 [L_\odot]
M_\star	0.45 ± 0.05 [M_\odot]
R_\star	0.43 ± 0.03 [R_\odot]

Notes. ^(†) Bakos et al. (2002).

orders have low signal-to-noise ratio (Díaz et al. 2007; da Silva et al. 2010). We compare GJ 3634 to a quiet (GJ 581 – Bonfils et al. 2005b) and a moderately active (GJ 176 – Forveille et al. 2009) M dwarf, and diagnose an intermediate level of activity (see Fig. 1). Also, its galactic velocities ($U = -35$, $V = -25$, $W = -20$ km s⁻¹ – Hawley et al. 1996) place GJ 3634 in a position between the young and old disks populations (Leggett 1992). Stars of this population have a probable age >3 Gyr (Haywood et al. 1997), which is consistent with the level of activity we estimate from the Na I doublet. Together with the low $v \sin i \lesssim 1$ km s⁻¹ we estimate from HARPS spectra, we expect that GJ 3634's magnetic activity is too low to affect our radial-velocity measurements, at least on short time scales.

3. Radial-velocity detection

3.1. Data and orbital analysis

We observed GJ 3634 with the HARPS spectrograph, the state-of-the-art velocimeter fiber-fed by the ESO/3.6-m telescope (Mayor et al. 2003; Pepe et al. 2004). Our setting remains the same as in our GTO program and we refer the reader to Bonfils et al. (2011), for a detailed description.

We started GJ 3634 observations by a single 300-s exposure on 2009 March 25. We verified that the target was neither a double-line spectroscopic binary, nor a fast rotator, and that the precision was sufficient for a planet search. Among other stars selected with a single measurement, we re-observed GJ 3634

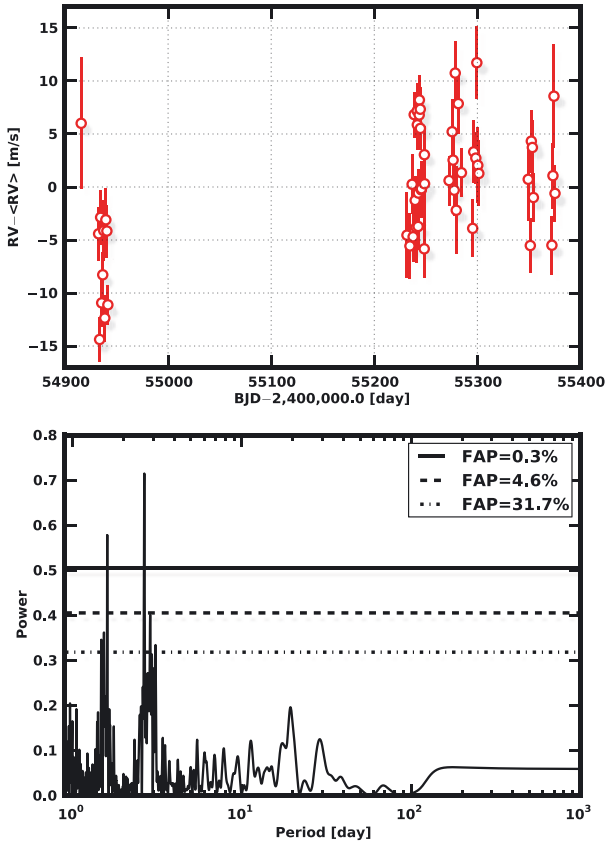


Fig. 2. *Upper panel:* RV time series of GJ 3634, collected in 2009 (Barycentric Julian Date < 2 455 198) and in 2010 (BJD > 2 455 198). *Bottom panel:* periodogram of GJ 3634 RVs collected in 2010. The horizontal lines show different levels of false-alarm probabilities.

about two weeks later with an exposure of 900 s. Sometimes, the two weeks lap time enables the identification of single-line spectroscopic binaries right after the second measurement, in which case we would discard the star from the target list. For GJ 3634 however, we continued the observations at a pace of one measurement per night during 10 consecutive nights, and with 900-s exposures.

After those observations, the dispersion of GJ 3634 RVs ($\sigma_e = 5.8$ m/s) appeared to be in excess of their estimated uncertainties ($\langle\sigma_i\rangle = 2.6$ m/s). Power excess could already be seen in the periodogram of those velocities at the periods 1.6 and 2.7 day (one-day aliased of each other), albeit with a modest false-alarm probability (FAP) of $\sim 4.3\%$. GJ 3634 nevertheless became a high-priority target for the next season and this year, we gathered 43 more measurements, which makes a total of 54 (Fig. 2 and Table 2).

A periodogram of this season’s velocities shows a clear power excess ($p_0 = 0.71$) around a 2.65-day period, plus a less powerful pic at the sidereal-day alias of this period, 1.60 day ($p = 0.58$). Shuffling the RVs but retaining the dates, we created 10 000 virtual data sets and computed their periodograms. The distribution of their maxima has a mean value of 0.29, with a standard deviation of 0.06. None of the maxima measured in the simulated periodograms is as high or higher than the power maxima measured on the periodogram of the original data, which suggests a FAP lower than $O(1/10\,000)$. We also computed an analytical estimate of the FAP with Cumming (2004)’s prescription: $FAP \simeq M \cdot (1 - p_0)^{(N-3)/2}$, where M is the

number of independent frequencies in the periodogram, p_0 its highest power value and N the number of measurements. We approximate M by the inverse of the time span of our observations and obtain the extremely low FAP value of $\sim 2.5 \times 10^{-9}$.

Still considering velocities from 2010 only, we performed a Keplerian fit, using the period of the detected signal as a starting guess. Our minimization converges toward a solution with a reduced $\chi_{\text{red}}^2 = 0.95 \pm 0.23$, greatly improved compared with the reduced $\chi_{\text{red}}^2 = 3.14 \pm 0.39$ of a fit by a constant.

Now considering all data from both 2009 and 2010, we subtracted that best fit to all velocities. We find that the RVs of 2009 have an average value ~ 8 m/s lower compared with those of 2010. This RV offset most likely betrays the presence of an additional companion around GJ 3634, though more data are required to complete the orbit and confirm this interpretation. The periodogram of all RVs taken together is actually dominated by the power of that long-term variation and, for a better legibility, we chose to restrict our periodogram analysis to the subset of the 2010 RVs.

Finally, we found that a planet plus a quadratic drift is a good model to describe all RVs. We use this model together with a Markov Chain Monte Carlo (MCMC) algorithm to perform a Bayesian analysis of all RVs (e.g. Gregory 2005, 2007; Ford 2005). For each parameter, we marginalize over all other parameters, take the median of the posterior density function as the optimal value, and the centered 68% interval as an error estimate. Our model was composed of nine parameters : the orbital period ($P = 2.6459 \pm 0.0006$ day), the semi-amplitude ($K_1 = 5.60 \pm 0.57$ m/s), the time of passage at periastron ($T = 2,454,917.04^{+0.82}_{-0.52}$), the orbital eccentricity ($e = 0.09^{+0.09}_{-0.06}$), the argument of periastron ($\omega = 100 \pm 71^\circ$), the slope ($\text{slope} = 21.1 \pm 2.8$ m/s/yr) and quadrature ($\text{quad} = -10.3 \pm 2.4$ m/s/yr²) of the long-term drift, and a jitter component ($\epsilon_j = 0.47^{+0.51}_{-0.35}$ m/s), quadratically co-added to the photon noise. We note that both e and ϵ_j are compatible with zero and give upper values $e < 0.31$ and $\epsilon_j < 1.8$ m/s, valid with a 99% confidence level.

The Bayesian approach also offers the possibility to evaluate the confidence level of our detection more rigorously. We thus ran MCMC chains for several models and computed their relative Bayes factor. We found that a model composed of *1 planet + a quadratic drift* is favored over a model composed of *a single planet* by a factor $\sim 5 \times 10^5$. And over a constant model (i.e. no planet and no drift), we found that *1 planet + a quadratic drift* model is favored by a factor of $\sim 1 \times 10^9$, which is in line with the very strong detection.

Finally, we show the optimal solution in Fig. 3, and using $M_\star = 0.45 \pm 0.05 M_\odot$ we convert the orbital parameters into a planetary minimum mass $m \sin i = 7.05 \pm 0.89 M_\oplus$.

3.2. Activity diagnostics

We compute the RVs of GJ 3634 by measuring the Doppler shifts of spectra recorded by the HARPS spectrograph. At first, the method assumes that the spectrum emerging from the stellar surface remains unchanged over time, except for the Doppler shifts attributed to one or more perturbing bodies that impose velocity changes on the star. Then, one has to consider the stellar phenomena able to alter the emergent spectrum. Spots and plages, for instance, can break the balance between the blue- and red-shifted halves of a rotating star. As the star rotates, the stellar inhomogeneities modulate the overall integrated spectrum and bias RV measurements. In some cases, the modulation can even mimic the Keplerian wobble expected from an orbiting planet,

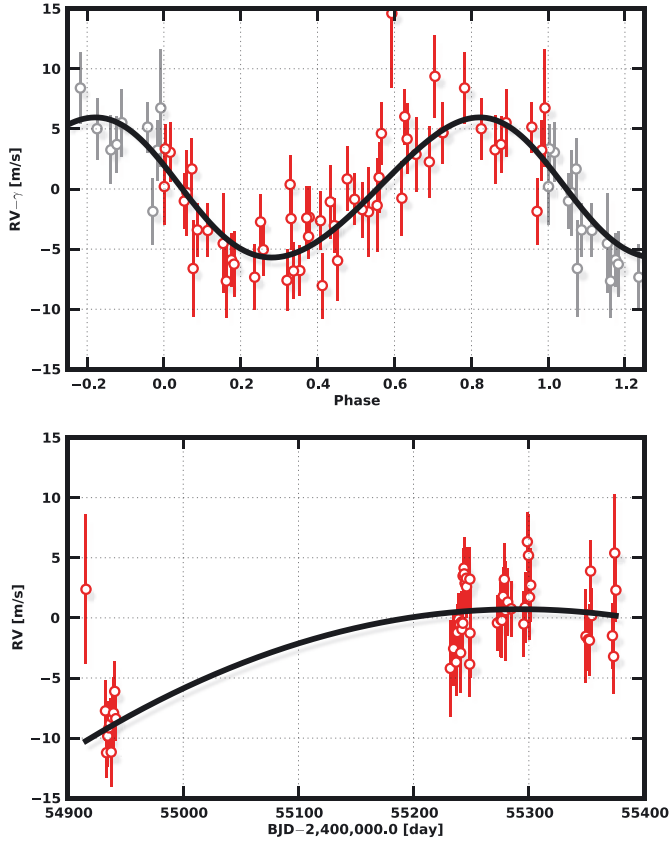


Fig. 3. Decomposition of our nominal orbital model for GJ3634. The top panel shows RVs with the contribution of the long-term drift subtracted and phased with the planet’s orbital period. The bottom panel shows RVs as a function of time, with the Keplerian contribution removed. Gray points duplicate some of the red points. The model is also decomposed and plotted with a solid curve in each panel.

like for GJ 674 (Bonfils et al. 2007). In our search for planets orbiting M dwarfs, the RV modulations we identified were actually more often caused by spots or plagues than planets (Bonfils et al. 2011).

Although GJ 3634’s low $v \sin i$ ($\lesssim 1 \text{ km s}^{-1}$) makes correspond an improbable inclination to a few-day rotational period, we applied several diagnostics to distinguish between stellar activity and true RV shifts. A first class of diagnostics is based on the spectral line asymmetry. We measure both the bisector-inverse slope (BIS) and the full-width at half-maximum (FWHM) of the cross-correlation function (an averaged spectral line of HARPS spectra). None seems to show any periodicity, nor a correlation with the radial velocities. This type of analysis however loses its power for low $v \sin i$. Alternatively, a second class of diagnostics is based on the photometric and spectral signatures of active regions of the stellar surface. Spots, plagues, and filaments produce back emission in Ca II H&K, Na I D and H α lines. We therefore also investigated the possible variation of indices based on these lines, but found no counterpart to the observed RV variation.

4. Transit search with *Warm Spitzer*

The a priori geometric probability that GJ 3634b transits its host star is $\sim R_*/a \simeq 7\%$. We therefore decided to follow-up on the detection of GJ 3634b with a photometric campaign, and part of

our RV observations aimed at refining the orbital ephemeris to narrow the probable transit-search window.

4.1. Light curve

For a rocky composition, the transit depth could be shallower than 1 mmag, making a ground-based transit detection extremely difficult. We therefore opted for the Infra-Red Array Camera (IRAC) onboard *Warm Spitzer* (Soifer et al. 2007; Fazio et al. 2004) and scheduled our observations to cover $\sim 2\sigma$ of the probable transit window, from 2010 July 12 17h50 UT to 2010 July 13 00h15 UT. We chose to observe in the 4.5- μm channel because it exhibits the lowest intrapixel-sensitivity variation. Indeed, combined with the low-frequency jitter of the telescope, this inhomogeneous response produces a strong correlation between the recorded flux and the position of the star on the detector (Knutson et al. 2008 and references therein). We used the established technique of continuous staring in non-dithered subarray mode with the longest exposure time for which the star would not be saturated on the detector (0.32 s).

Our data consist of 845 blocks of 64 individual subarray images. We used the Basic Calibrated Data (BCD) produced by the *Spitzer* standard pipeline (version S18.18.0) and, after conversion from specific intensity (MJy/sr) to photon counts, we obtained aperture photometry in each subarray image using the IRAF/DAOPHOT¹ software (Stetson 1987). We determined the stellar position by fitting a Gaussian profile to the stellar image, and obtained our best results with an aperture of 3.5 pixels. In each image we subtracted a mean sky-background measured in an annulus extending from 12 to 15 pixels from the aperture center. For each block of 64 subarray images, we discarded the discrepant values for the measurements of flux, background, and the x - and y -positions using a 10- σ median clipping, and averaged the remaining values. Only 0.3% of the measured fluxes were discarded. To estimate the error on the averaged value we chose to divide the rms of the block by the squared root of the number of measurements we kept. Figure 4 shows the evolution of the measured flux and position time series. It clearly shows the correlation of the photometry with the stellar position, which leads to a correlated noise at the level of a few mmags in the light curve. It also shows that the flux decreased sharply during the first 5 min of the run, and this drop is correlated with a sharp variation of the y -position. We decided to discard these first 5 min (13 measurements) from our analysis, and accordingly obtained a final light curve with 832 measurements.

The flux-position correlation is well described by a quadratic polynomial in x and y :

$$A(dx, dy, t) = a_1 + a_2 dt + a_3 dx + a_4 dx^2 + a_5 dy + a_6 dy^2 + a_7 dx dy, \quad (1)$$

where dx and dy are the distance of the PSF center to the center of the pixel, and dt is the time elapsed since 15 min before the start of the run. Detrending the light curve by this seven-parameter function leads to a time-series nearly free of correlated noise (see Fig. 5 and Table 3*). The rms is 611 ppm, much similar to the mean individual error (~ 616 ppm) and once binned per 20 min, the rms decreases to 100 ppm.

¹ IRAF is distributed by the National Optical Astronomy Observatory, which is operated by the Association of Universities for Research in Astronomy, Inc., under cooperative agreement with the National Science Foundation.

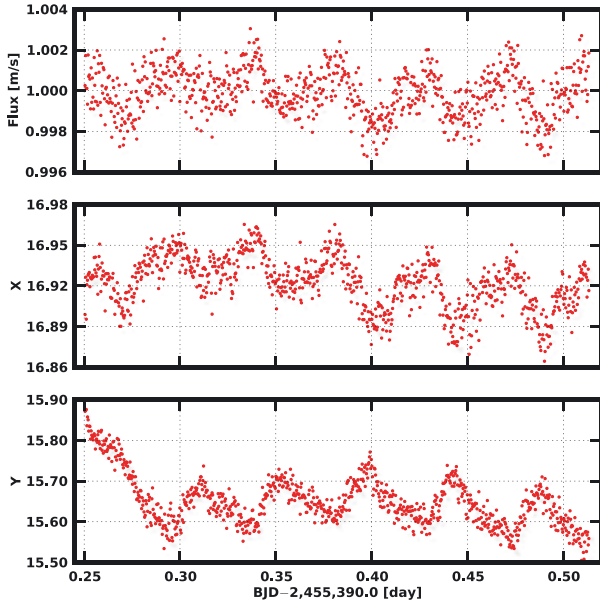


Fig. 4. *Top:* Raw $4.5\ \mu\text{m}$ *Warm Spitzer* light curve for GJ 3634. *Middle and bottom:* evolution of x - and y -positions of the PSF center during the run.

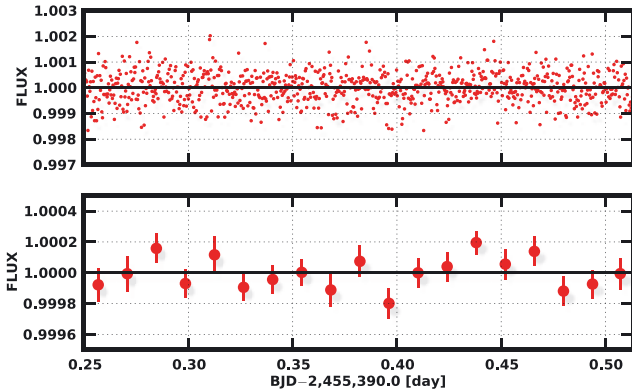


Fig. 5. *Top:* $4.5\ \mu\text{m}$ light curve detrended by the baseline function $A(dx, dy, dt)$ (see Eq. (1)). *Bottom:* same light curve binned per 20 min time bins.

4.2. Orbital analysis

To determine the *posterior* transit probability of GJ 3634b, we pooled the radial-velocity and the photometry and applied another Bayesian analysis using MCMC. This analysis closely follows those presented for HD 40307b and CoRoT-2b (Gillon et al. 2010), and we refer the reader to these for details regarding the choice of parameters and their priors. To briefly recall, the model includes a planet on a Keplerian orbit, a quadratic RV drift, a photometric baseline, and the stellar mass and radius. At each step of the Markov chain a set of parameters is proposed and, to accept (or reject) the proposal, we evaluate the joint likelihood of the data (RV+photometry) and the parameters. The planet’s parameters act on the radial-velocity likelihood and, if transiting, on the photometry likelihood. The parameters of the quadratic drift and the stellar mass affect only the RV likelihood, and the baseline and the stellar radius only the photometry likelihood.

To improve the efficiency of convergence, we decoupled the linear parameters (the photometric baseline, the RV trend, and the gamma velocity) from the MCMC and fitted them with a least-square minimization. More precisely, the quadratic drift counts two parameters (the *slope* and the *curvature*) and the photometric baseline counts seven (Eq. (1)). We also describe the planet with the following eight parameters: the orbital period P , $\sqrt{e} \cos \omega$ and $\sqrt{e} \sin \omega$, where e and ω are the eccentricity and argument of periastron, a parameter $K_2 = K \sqrt{1 - e^2} P^{1/3}$ to replace the RV semi-amplitude K , the time T_{tr} (when the true anomaly $\nu = \pi/2 - \omega$), the impact parameter $b' = a \cos i / R_*$ and the planetary radius R_p chosen between $1.2 R_{\oplus}$ for a pure-iron planet (Seager et al. 2007) and an arbitrary upper limit of $12 R_{\oplus}$. The stellar mass and radius are the only parameters with non-uniform priors; they are drawn randomly at each step of the Markov chain following their normal distributions, $N(0.45, 0.05^2) M_{\odot}$ and $N(0.43, 0.03^2) R_{\odot}$. Note finally that we chose not to include a description of the stellar limb darkening, nor of the Rossiter-McLaughlin anomaly, because both are expected to be small.

We ran the analysis in two steps. First, we performed a Markov chain of 500 000 steps to assess the level of correlated noise in the photometry and the jitter noise in the RVs. We found that no jitter noise is required for the RVs while we multiplied the photometric error by $\beta_{\text{red}} = 1.07$ (e.g. Gillon et al. 2010). Then, we performed a new chain of 500 000 steps with updated errors. Our MCMC converges on a statistical description of possible solutions. We marginalized the posterior distribution of each parameters and calculated their median values and 68.3% intervals (Table 4). Among the solutions, none corresponds to a detected transit, and among all configurations with a transit, 92% are rejected. Only few transit configurations remain unexplored (Fig. 6), and the posterior transit probability decreases to 0.9% (and even to 0.5% if only total transits are retained).

This global analysis also improves the measurement of orbital parameters. Indeed, the small subset of transit configurations that are inconsistent with the photometry removes as many orbital inclinations – and therefore planetary masses – from the possible solutions. It thus provides a statistical description for the true mass of GJ 3634b ($m_p = 8.4^{+4.0}_{-1.5} M_{\oplus}$).

5. Residuals and detection limits

At this point, we identified the Keplerian motion induced by a super-Earth, searched for its possible transit and were able to reject most transit configurations. We also identified a second signal that most probably corresponds to the incomplete orbit of a companion of whose true nature is yet unknown. The data of 2010 are weakly sensitive to that signal, suggesting an orbital period greater than their time span (>200 d), and a mass $\gtrsim 32 M_{\oplus}$ ($\sim 2 M_{\text{Nep}}$).

The habitable zone of GJ3634 is located between ~ 0.12 and ~ 0.33 AU from the star, corresponding to orbital periods from ~ 22 to 104 d. There is therefore much interest in characterizing our sensitivity in the period range below 200 d. Figure 7 shows the RV residuals once the best fit for the *1 planet + quadratic drift* model has been removed. They have a dispersion $\sigma = 2.32$ m/s. The reduced $\chi^2 = 1.00 \pm 0.10$ of the solution suggests the remaining dispersion is explained by the measurement uncertainties and argues against more complex models. The periodogram of the residuals (Fig. 7, bottom panel) does not display significant power excess. The most important pic however is located at a period ~ 19 d (FAP = 10%), close to the habitable

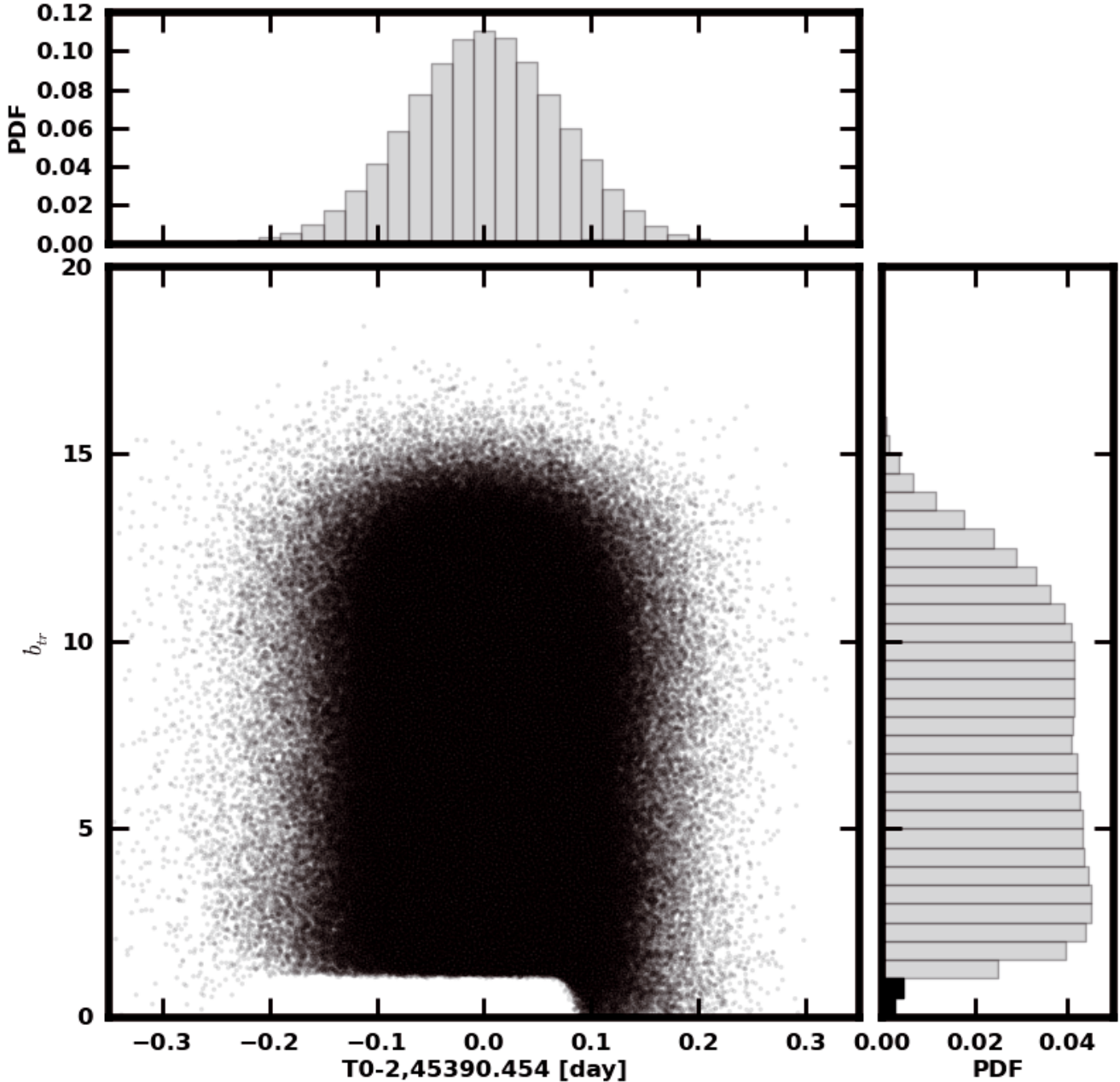


Fig. 6. Joint marginal posterior distribution of T_0 (transit timing) and b_{tr} (transit impact parameter) $= (a \cos i/R_*)[(1 - e^2)/(1 + e \sin(\omega))]$. Full transit configurations represent 0.5% of the PDF and are shown in black in the histograms.

zone's inner edge, and will retain our attention when more RVs will be collected.

We then turn to assess which planets, as a function of minimum mass and orbital period, are rejected given the residuals. Because the model to describe the long-term variation is uncertain, we restrict our analysis to periods ≤ 200 d. We use a method applied by [Cumming et al. \(1999, 2008\)](#) and [Zechmeister & Kürster \(2009\)](#), which we recently employed to derive detection limits of 85 M dwarfs from our sample ([Bonfils et al. 2011](#)). In brief, we carried out bootstrap resampling of the residuals, generated 1000 virtual data sets, and computed their periodograms. We used the 1000 periodograms to build an empirical power distribution, scan the periods and determine the threshold that encompasses 99% of the power realizations. We then injected

faked circular orbits in the observed residuals (with 12 different phases), and increased their semi-amplitude until they produced a power as high or higher than our power threshold in the periodogram (for all trial phases). This semi-amplitude is the level above which a planet can be conservatively rejected (with a confidence level of 99%). Finally, we converted this limit in a minimum-mass limit using Kepler's law and our estimate of the stellar mass ([Fig. 8](#)). To aid the reader, we also report in [Fig. 8](#) the putative habitable zone, following the [Selsis et al. \(2007\)](#)'s prescription.

The detection limit shows that we rule out additional planets more massive than $>10 M_{\oplus}$ up to periods well above 10 d, except for a very narrow period range around 2 d, where our sensitivity decreases because of the observation sampling. In

Table 4. Median and 1- σ limits of the marginal posterior distributions of the orbital parameters.

Parameter	Value + errors	Units
Jump parameters		
$dF = (R_p/R_*)^2$	0.020 ± 0.012	
$b' = a \cos(i)/R_*$	7.5 ± 4.3	R_*
Transit epoch $T_0 - 2\,450\,000$	5390.454 ± 0.073	BJD
Orbital period P	2.64561 ± 0.00066	days
$K_2 = K \sqrt{1 - e^2} P^{1/3}$	7.68 ± 0.75	
$\sqrt{e} \cos \omega$	$-0.04^{+0.20}_{-0.19}$	
$\sqrt{e} \sin \omega$	$0.17^{+0.19}_{-0.24}$	
RV baseline parameters		
Systemic RV	$5.18635^{0.00015}_{-0.00016}$	km s^{-1}
Slope	21.77 ± 0.77	m/s/yr
Curvature	-11.62 ± 0.77	m/s/yr^2
Deduced parameters		
RV K	5.59 ± 0.55	m/s
Orbital semi-major axis a	$0.0287^{+0.0010}_{-0.0011}$	AU
Orbital inclination i	59^{+18}_{-24}	deg
Orbital eccentricity e	$0.080^{+0.094}_{-0.057}$	
Upper limit to e (99%)	<0.36	
Argument of periastron ω	84^{+52}_{-130}	deg
$M_p \sin i$	$7.0^{+0.9}_{-0.8}$	M_\oplus
M_p	$8.4^{+4.0}_{-1.5}$	M_\oplus
Eclipse probabilities		
P_{transit}	0.9%	
$P_{\text{fulltransit}}$	0.5%	
$P_{\text{occultation}}$	0.7%	
$P_{\text{fulloccultation}}$	0.4%	

GJ3634's habitable zone, we exclude planets more massive than $m \sin i \sim 8\text{--}20 M_\oplus$, from the inner to the outer edges.

6. Conclusion

We report the detection of a $m \sin i = 7.0^{+0.9}_{-0.8} M_\oplus$ planet orbiting the nearby M dwarf GJ 3634. We followed-up on the RV detection with IRAC/*Spitzer* photometry to check whether the planet could be seen to transit its parent star. Our light curve confidently rejects most of the orbital configurations corresponding to a transiting planet as the posterior probability for full transit is decreased to $\sim 0.5\%$.

That detection adds to the handful of low-mass Neptunes and super-Earths detected so far. About a dozen planets are known with $m \sin i \lesssim 8 M_\oplus$ and almost half orbit M dwarfs. Among those, the transiting GJ 1214b has a similar mass ($m \sin i = 6.55 \pm 0.98 M_\oplus$ – Charbonneau et al. 2009) as GJ 3634b. GJ 1214b is found to have a thick atmosphere and, in structure and composition, resembles more a Neptune-like planets than a large rocky planet. It has also been suggested that, if this characteristic is shared by habitable super-Earths detected in RV surveys, the extreme pressure and the absence of stellar radiation at the surface of the planet would render them inhospitable for life as we know it. This large atmosphere however may result

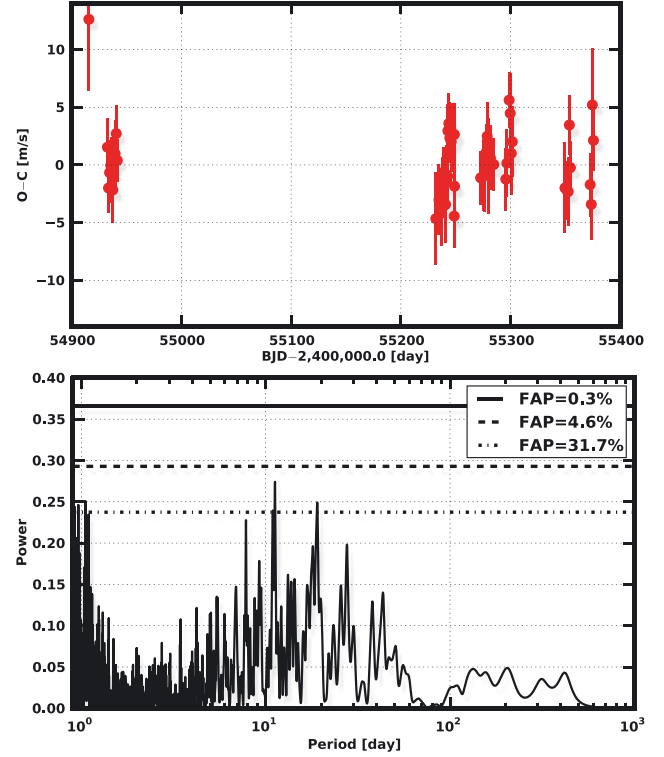


Fig. 7. Upper panel: RV residuals around the best solution for a 1 planet + quadratic drift model. Bottom panel: periodogram of the residuals.

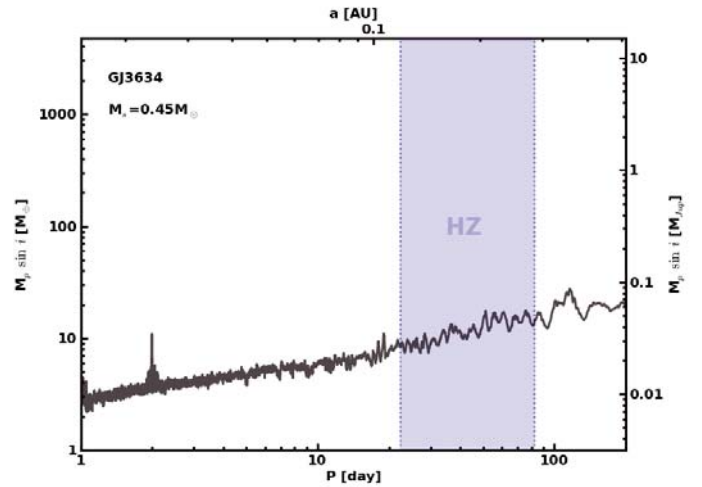


Fig. 8. Detection limit imposed by RVs residuals around the best solution for a 1 planet + quadratic drift model, for periods <200 d. The light blue area delineates the habitable zone, using Venus and early-Mars criteria (Selsis et al. 2007).

from the bias to detect larger planets inherent to photometric search or simply to the large variety of planets. The bias of transit searches driven by RV observations is toward more massive rather than bigger planets. As a result, they may provide candidates with structure and composition much different from those the photometric-search finds.

Acknowledgements. We thank the anonymous referee for his careful reading and suggestions. M.G. is FNRS Research Associate. N.C.S., V.N. and I.B. acknowledge the support by the European Research Council/European Community under the FP7 through a Starting Grant, as well as in the form of grants reference PTDC/CTE-AST/098528/2008, PTDC/CTE-AST/098604/2008 and SFRH/BD/60688/2009, funded by Fundação para a Ciência e a Tecnologia

(FCT), Portugal. NCS would further like to thank the support from FCT through a Ciência 2007 contract funded by FCT/MCTES (Portugal) and POPH/FSE (EC).

References

- Bakos, G. Á., Sahu, K. C., & Németh, P. 2002, *ApJS*, 141, 187
- Baraffe, I., Chabrier, G., Allard, F., & Hauschildt, P. H. 1998, *A&A*, 337, 403
- Bonfils, X., Delfosse, X., Udry, S., et al. 2005a, *A&A*, 442, 635
- Bonfils, X., Forveille, T., Delfosse, X., et al. 2005b, *A&A*, 443, L15
- Bonfils, X., Mayor, M., Delfosse, X., et al. 2007, *A&A*, 474, 293
- Bonfils, X., Delfosse, X., Udry, S., Forveille, & T., Mayor, M. 2011, *A&A*, submitted
- Charbonneau, D., Brown, T. M., Burrows, A., & Laughlin, G. 2007, *Protostars and Planets V*, 701
- Charbonneau, D., Berta, Z. K., Irwin, J., et al. 2009, *Nature*, 462, 891
- Cumming, A. 2004, *MNRAS*, 354, 1165
- Cumming, A., Marcy, G. W., & Butler, R. P. 1999, *ApJ*, 526, 890
- Cumming, A., Butler, R. P., Marcy, G. W., et al. 2008, *PASP*, 120, 531
- da Silva, J. G., Santos, N. C., & Bonfils, X. 2010 [[arXiv:1012.3640](https://arxiv.org/abs/1012.3640)]
- Delfosse, X., Forveille, T., Ségransan, D., et al. 2000, *A&A*, 364, 217
- Díaz, R. F., Cincunegui, C., & Mauas, P. J. D. 2007, *MNRAS*, 378, 1007
- Eggen, O. J. 1987, *A. J.*, 93, 379
- Fazio, G. G., Hora, J. L., Allen, L. E., et al. 2004, *ApJSS*, 154, 10
- Ford, E. B. 2005, *A. J.*, 129, 1706
- Forveille, T., Bonfils, X., Delfosse, X., et al. 2009, *A&A*, 493, 645
- Forveille, T., Bonfils, X., Curto, G. L., et al. 2011, *A&A*, 526, A141
- Gillon, M., Pont, F., Demory, B.-O., et al. 2007, *A&A*, 472, L13
- Gillon, M., Lanotte, A. A., Barman, T., et al. 2010, *A&A*, 511, 3
- Gregory, P. C. 2005, *AJ*, 631, 1198
- Gregory, P. C. 2007, *MNRAS*, 374, 1321
- Hawley, S. L., Gizis, J. E., & Reid, I. N. 1996, *AJ*, 112, 2799
- Haywood, M., Robin, A. C., & Creze, M. 1997, *A&A*, 320, 428
- Johnson, J. A., & Apps, K. 2009, *AJ*, 699, 933
- Kasting, J. F., Whitmire, D. P., & Reynolds, R. T. 1993, *Icarus*, 101, 108
- Leggett, S. K. 1992, *ApJSS*, 82, 351
- Mayor, M., Pepe, F., Queloz, D., et al. 2003, *The Messenger*, 114, 20
- Mayor, M., Bonfils, X., Forveille, T., et al. 2009, *A&A*, 507, 487
- Pepe, F., Mayor, M., Queloz, D., et al. 2004, *A&A*, 423, 385
- Riedel, A. R., Subasavage, J. P., Finch, C. T., et al. 2010, *AJ*, 140, 897
- Schlaufman, K. C., & Laughlin, G. 2010, *A&A*, 519, 105
- Seager, S., Kuchner, M., Hier-Majumder, C. A., & Militzer, B. 2007, *AJ*, 669, 1279
- Selsis, F., Kasting, J. F., Levrard, B., et al. 2007, *A&A*, 476, 1373
- Skrutskie, M. F., Cutri, R. M., Stiening, R., et al. 2006, *AJ*, 131, 1163
- Soifer, B. T., Carey, S., Helou, G., et al. 2007, *BAAS*, 211, 788
- Stetson, P. B. 1987, *ASP*, 99, 191
- Udry, S., Bonfils, X., Delfosse, X., et al. 2007, *A&A*, 469, L43
- Zechmeister, M., & Kürster, M. 2009, *A&A*, 496, 577